

Geometric optimal control of the contrast imaging problem in Nuclear Magnetic Resonance

B. Bonnard*, O. Cots, S. J. Glaser†, M. Lapert, D. Sugny‡ and Y. Zhang

October 19, 2018

Abstract

The objective of this article is to introduce the tools to analyze the contrast imaging problem in Nuclear Magnetic Resonance. Optimal trajectories can be selected among extremal solutions of the Pontryagin Maximum Principle applied to this Mayer type optimal problem. Such trajectories are associated to the question of extremizing the transfer time. Hence the optimal problem is reduced to the analysis of the Hamiltonian dynamics related to singular extremals and their optimality status. This is illustrated by using the examples of cerebrospinal fluid / water and grey / white matter of cerebrum.

1 Introduction

In a series of recent articles [2, 5, 6, 7, 26, 29], geometric optimal control combined with adapted numerical schemes such as the HamPath code [14] is used to analyze the optimal control of Kossakowsky-Lindblad equations [1, 13, 21]. These equations describes the evolution of a two-level dissipative quantum system whose dynamics is governed by a three-dimensional system

$$\begin{aligned}\frac{dx}{dt} &= -\Gamma x + u_2 z \\ \frac{dy}{dt} &= -\Gamma y - u_1 z \\ \frac{dz}{dt} &= \gamma_- - \gamma_+ z + u_1 y - u_2 x,\end{aligned}\tag{1}$$

the state variable $q = (x, y, z)$ belonging to the Bloch ball $|q| \leq 1$ which is invariant for the dynamics since the dissipative parameters $\Lambda = (\Gamma, \gamma_+, \gamma_-)$ satisfy $2\Gamma \geq \gamma_+ \geq |\gamma_-|$. The control field is $u = (u_1, u_2)$. The underlying

*Institut de Mathématiques de Bourgogne, UMR CNRS 5584, 9 Avenue Alain Savary, BP 47 870 F-21078 DIJON Cedex FRANCE

†Department of Chemistry, Technische Universität München, Lichtenbergstrasse 4, D-85747 Garching, Germany

‡Laboratoire Interdisciplinaire Carnot de Bourgogne (ICB), UMR 5209 CNRS-Université de Bourgogne, 9 Av. A. Savary, BP 47 870, F-21078 DIJON Cedex, FRANCE, dominique.sugny@u-bourgogne.fr

optimal control problem consists of minimizing the transfer time with a bound on the modulus of the control or of minimizing the energy transfer $\int_0^T |u|^2 dt$ with a fixed control duration.

Such a system is a model for the control of a molecule in a dissipative environment using a laser field [22, 27] but also in Nuclear Magnetic Resonance (NMR) spectroscopy where the dynamics of a spin 1/2 particle can be described, up to a renormalization, by the Bloch equation which is of the form (1) with the restriction $\gamma_- = \gamma_+$ [11, 15, 20]. This implies that in this model, the equilibrium point of the free motion is the north pole $(0, 0, 1)$ of the Bloch ball.

In NMR, we also recall that the control is a transverse radio-frequency magnetic field in the (x, y) - plane, a constant magnetic field being applied in the z -direction. In this domain, a striking application of geometric optimal control was a gain of 60 % in the control duration of the saturation of a spin 1/2 particle [19]. The saturation problem consists in bringing the magnetization vector of the sample from the equilibrium point to the center of the Bloch ball [8]. Such a control can be achieved by a standard NMR technique, the inversion recovery sequence, composed of a bang arc to invert the magnetization vector and a singular one along the vertical z - axis to reach the target state. It can be shown that the geometric time-optimal solution is the concatenation of a bang, a horizontal singular arc, a bang and a final vertical singular arc. The gain in the control duration has been shown experimentally in [19]. The experiments were performed using the proton spins of H_2O in an organic solvent at room temperature. This result shows that the optimized pulse sequence can really be implemented with modern NMR spectrometers and a reasonable match between theory and experiments.

Also this result is crucial because it confirms the ubiquity of singular trajectories in the optimal control of nonlinear systems [4]. In the preceding example, contrary to the apparent simplicity of the equations, the physical situation is non trivial due to the two singular directions which are necessary to compute the optimal solution. A direct generalization of this problem is the one of the contrast in NMR imaging. The model is obtained by considering two uncoupled spins, each of them being solution of the Bloch equations (1) with different damping coefficients $\Lambda_1 = (\Gamma_1, \gamma_1)$, $\Lambda_2 = (\Gamma_2, \gamma_2)$, but controlled by the same magnetic field. Denoting each system by

$$\frac{dq_i}{dt} = F_i(q_i, \Lambda_i, u)$$

where $q_i = (x_i, y_i, z_i)$ is the magnetization vector of each spin particle, this leads to a system written shortly as

$$\frac{dx}{dt} = F(x, u)$$

where $x = (q_1, q_2)$. The associated optimal control problem is the following: Starting from the equilibrium point of the dynamics $x_0 = ((0, 0, 1), (0, 0, 1))$, the goal is to reach in a given transfer time T (which can be fixed or not), the final state $q_1(T) = 0$ for the first spin while maximizing a cost $C(q_2(T))$ (e.g. $|q_2(T)|^2$ or the projection of $q_2(T)$ on one axis). A subcase of this problem is to restrict the system to $x_1 = x_2 = 0$ by considering only the component u_1 of the control field. Our aim in this paper is to present a geometric study of this

control problem based on the analysis of the Hamiltonian dynamics given by the Pontryagin Maximum Principle (PMP) [23], the optimal control problem being a standard Mayer problem.

An important point in our analysis will be the introduction of singular trajectories of the system $\frac{dx}{dt} = F(x, u)$ whose control domain N is a smooth submanifold of \mathbb{R}^p defined as follows (one can assume that $N = \mathbb{R}^p$):

Definition 1 *A control $u \in L^\infty([0, T])$ is called singular on $[0, T]$ if the derivative of the extremity mapping $E^{x_0, T} : u \in L^\infty \mapsto x(T, x_0, u)$, where $x(\cdot)$ denotes the response to $u(\cdot)$ initiating from x_0 at $t = 0$, is not of full rank.*

This definition is not the standard definition in the engineering literature, in particular it depends upon the control domain. But it is the correct mathematical definition in optimal control since optimality is related to openness properties of the extremity mapping.

A large amount of work has been done recently in control theory to analyze the role of singular extremals. This can be summarized as follows:

1. They are feedback invariant.
2. They can be computed using the PMP as solutions of

$$\dot{x} = \frac{\partial H}{\partial p}, \quad \dot{p} = -\frac{\partial H}{\partial x}, \quad \frac{\partial H}{\partial u} = 0$$

where $H(x, p, u) = \langle p, F(x, u) \rangle$ is the Hamiltonian lift of the system.

As such they are extremal solutions of any Mayer type problem associated to a system where the cost and the boundary conditions only give boundary conditions. Also recent works have shown how to compute their first conjugate time, that is the first time such that the extremity mapping becomes open. This time corresponds also to the time where the trajectories lose their local optimality. Theoretically, it is related to the concept of singularity of Lagrangian manifolds [4] and is numerically implemented in the Hampath code [14].

Hence going back to the contrast imaging problem, a research program is to analyze the Hamiltonian dynamics of the singular extremals completed by numerical simulations to compute the optimal solutions. This is a difficult task since the problem is depending upon different relaxation parameters in the Bloch equation. In this paper, we will present the geometric tools and some preliminary numerical results in two particular cases by considering only one component of the control field.

The organization of this article is the following. In the first section, the Maximum Principle is introduced to select minimizers among extremal solutions in a Mayer problem. The role of singular extremals is presented and their optimality status is determined using the concept of conjugate points. In a second section, a thorough analysis of the geometric control of a single spin 1/2 particle is presented and it plays for specific values of the parameters, an important role in the problem. In the final section, we numerically analyze the geometry of singular extremals in view of studying some specific cases in NMR. Numerical computations of the optimal solution are also presented for two regularized cost functionals.

2 Geometric optimal control

2.1 Preliminaries

One considers a Mayer problem given by the following data :

1. A smooth system $\frac{dx}{dt} = F(x, u)$, $x \in \mathbb{R}^n$ with fixed initial state x_0 and a transfer time T , the controls being the set $\mathcal{U} = L^\infty([0, T], U)$ of bounded measurable mappings valued in a control domain $U \subset \mathbb{R}^p$.
2. A terminal manifold M defined by $f(x) = 0$ where $f : \mathbb{R}^n \rightarrow \mathbb{R}^k$ is a smooth mapping.
3. A cost to minimize : $\min_{u(\cdot) \in \mathcal{U}} C(q(T))$ where $C : \mathbb{R}^n \rightarrow \mathbb{R}$ is a smooth regular mapping.

The geometric setting is the following. Denote $x(t, u)$ the trajectory initiating from x_0 and associated to u , $A(x_0, T) = \cup_{u \in \mathcal{U}} x(T, u)$ the accessibility set at time T and introducing the manifold $C_m = \{f = 0, C(x) = m\}$ where m is a parameter, an optimal control u^* is such that $x^*(T) = x(T, u^*)$ belongs to the boundary of $A(x_0, T)$, $f(x^*(T, u^*)) = 0$ and m is minimum.

2.2 Pontryagin Maximum Principle

The application of the maximum principle leads to the following necessary conditions [23].

Proposition 1 *Let $u^*(\cdot)$ be an admissible control whose corresponding trajectory $x^*(t) = x(t, u^*)$ is optimal. Then there exists an absolutely continuous vector function $p^*(\cdot)$ and a scalar $p_0 \leq 0$ such that if we denote by H the pseudo-Hamiltonian $H(x, p, u) = \langle p, F(x, u) \rangle$, the following necessary conditions are satisfied a.e. on $[0, T]$:*

$$\frac{dx^*}{dt} = \frac{\partial H}{\partial p}(x^*, p^*, u^*), \quad \frac{dp^*}{dt} = -\frac{\partial H}{\partial x}(x^*, p^*, u^*) \quad (2)$$

$$H(x^*, p^*, u^*) = \max_{u \in U} H(x^*, p^*, u) \quad (3)$$

together with the boundary conditions:

$$f(x^*(T)) = 0 \quad (4)$$

$$p^*(T) = p_0 \frac{\partial C}{\partial x}(x^*(T)) + \langle \xi, \frac{\partial f}{\partial x}(x^*(T)) \rangle, \quad (5)$$

$\xi \in \mathbb{R}^k$, $p_0 \leq 0$ (transversality conditions).

Definition 2 *We call extremals a triplet (x, p, u) solution of (2) and of the maximization condition (3). It is called a BC- extremal if it satisfies the boundary conditions (4) and (5).*

2.3 A review of the properties of singular trajectories

Next we present some concepts and properties about singular trajectories which are important in our analysis, see [4] for a complete presentation.

We have the following characterization of singular control which allows a practical computation.

Proposition 2 *The control $u(\cdot)$ and the corresponding trajectory $x(\cdot)$ are singular on $[0, T]$ if and only if there exists a non zero adjoint vector $p(\cdot)$ such that (x, p, u) is solution a.e. on $[0, T]$ of*

$$\dot{x} = \frac{\partial H}{\partial p}, \quad \dot{p} = -\frac{\partial H}{\partial x}, \quad \frac{\partial H}{\partial u} = 0 \quad (6)$$

where $H(x, p, u) = \langle p, F(x, u) \rangle$ is the Hamiltonian lift. Moreover for each $0 < t \leq T$, $p(t)$ is orthogonal to $\text{Im}E'^{x_0, t}(u|_{[0, t]})$.

Definition 3 *A singular extremal is a triple (x, p, u) solution of the above equations. It is called:*

1. *Regular if $\frac{\partial^2 H}{\partial u^2}$ is of maximal rank.*
2. *Strongly normal if for each $0 < t_1 < t_2 \leq T$, $\text{Im}E'^{x(t_1), t_2-t_1}(u|_{[t_1, t_2]})$ is of corank one.*
3. *Exceptional if $H = 0$.*

Computation in the regular case: Using the condition $\frac{\partial^2 H}{\partial u^2} \neq 0$, one can solve locally the equation $\frac{\partial H}{\partial u} = 0$ and compute the singular control as a function $\hat{u}(z)$, $z = (x, p)$ and plugging such \hat{u} in H defines a true Hamiltonian denoted again $H(z)$. If Π is the standard projection $(x, p) \mapsto x$, one can define the exponential mapping $\exp_{x_0} : (t, p) \mapsto \Pi(\exp[t\vec{H}(x_0, p)])$ where x_0 is fixed. This leads to the following definition.

Definition 4 *Let $z(t) = (x(t), p(t))$ be the reference extremal solution of \vec{H} . The time t_c is said to be geometrically conjugate if \exp_{x_0} is not of maximal rank at $(t_c, p(0))$.*

We have the following standard test:

Proposition 3 *The time t_c is geometrically conjugate if and only if there exists a non trivial Jacobi field $J(t)$ solution of the variational equation $\delta\dot{z} = d\vec{H}(z(t))\delta z$ and vertical at time 0 and t_c : $d\Pi(J(0)) = d\Pi(J(t_c)) = 0$.*

The following result is crucial in our optimality analysis:

Proposition 4 *In the strongly normal case and in the non exceptional situation, the extremity mapping $E^{x_0, T}$ is open for the L^∞ - topology at $u|_{[0, t]}$ where $t > t_{1c}$.*

Application: One consider a control system of the form $F(x, u) = F_0(x) + u_1 F_1(x) + u_2 F_2(x)$ where the control domain U is the disk $u_1^2 + u_2^2 \leq 1$. The Hamiltonian is $H = H_0 + u_1 H_1 + u_2 H_2$ where $H_i = \langle p, F_i(x) \rangle$. The maximization condition (3) leads to

$$u_i = \frac{H_i}{\sqrt{H_1^2 + H_2^2}}, \quad i = 1, 2 \quad (7)$$

outside the switching surface Σ : $H_1 = H_2 = 0$. The corresponding extremals are called of order zero and there are solutions of the smooth vector field defined by $H(z) = H_0 + \sqrt{H_1^2 + H_2^2}$. The corresponding solutions are regular singular extremals if one restricts the control domain to the unit sphere S^1 . Introducing $u_1 = \cos \alpha$, $u_2 = \sin \alpha$ and extending the system using $\dot{\alpha} = v$, they correspond to singular trajectories of the extended system:

$$\dot{x} = F_0 + \cos \alpha F_1 + \sin \alpha F_2, \quad \dot{\alpha} = v.$$

The case of affine systems: For optimality analysis, one restricts our study to a single input affine system: $\dot{x} = F_0 + u_1 F_1$, $|u_1| \leq 1$. Relaxing the control bound, singular trajectories are parameterized by the constrained Hamiltonian system:

$$\dot{x} = \frac{\partial H}{\partial p}, \quad \dot{p} = -\frac{\partial H}{\partial x}, \quad \frac{\partial H}{\partial u_1} = H_1 = 0.$$

The singular extremals are not regular and the constraint $H_1 = 0$ has to be differentiated along an extremal to compute the controls. Introducing the Lie brackets of two vector fields X, Y computed with the convention

$$[X, Y](x) = \frac{\partial X}{\partial x}(x)Y(x) - \frac{\partial Y}{\partial x}(x)X(x),$$

and related to the Poisson bracket of the Hamiltonian lifts H_X, H_Y by the rule $\{H_X, H_Y\} = H_{[X, Y]}$, one gets:

$$H_1 = \{H_1, H_0\} = \{\{H_1, H_0\}, H_0\} + u_1 \{\{H_1, H_0\}, H_1\} = 0.$$

A singular extremal such that $\{\{H_1, H_0\}, H_1\} \neq 0$ is called of minimal order and the corresponding control is given by

$$u_{1s} = -\frac{\{\{H_1, H_0\}, H_0\}}{\{\{H_1, H_0\}, H_1\}}. \quad (8)$$

Plugging such u_{1s} into H defined a true Hamiltonian, whose solutions initiating from $H_1 = \{H_1, H_0\} = 0$ defined the singular extremals of order zero. They are related to the regular case using the following Goh transformation. Assuming F_1 non zero, then there exists a coordinate system (x_1, x_2, \dots, x_n) on an open set V such that $F_1 = \frac{\partial}{\partial x_n}$ and the system splits into:

$$\dot{x}' = F'(x', x_n), \quad \dot{x}_n = F_0'(x') + u_1$$

where $x' = (x_1, \dots, x_{n-1})$ and the system F' defined on an open subset V' where x_n is taken as the control variable is called the reduced system. We introduce the reduced Hamiltonian $H'(x', p', x_n) = \langle p', F'(x', x_n) \rangle$. One has:

$$\frac{\partial}{\partial t} \frac{\partial H}{\partial u} = \{H_1, H_0\} = -\frac{\partial H'}{\partial x_n} \quad (9)$$

$$\frac{\partial}{\partial u} \frac{\partial^2 H}{\partial t^2} \frac{\partial H}{\partial u} = \{\{H_1, H_0\}, H_1\} = -\frac{\partial^2 H'}{\partial x_n^2}. \quad (10)$$

This gives the relation between the affine singular case and the regular one.

2.4 High-order maximum principle in the affine case

As a consequence and using the generalized Legendre Clebsch condition deduced from the high-order maximum principle [17], one gets the following.

Consider the Mayer problem for an affine system of the form $\dot{x} = F_0(x) + u_1 F_1(x)$, $|u_1| \leq 1$. Then the following conditions are necessary for optimality:

$$\begin{aligned} \dot{x} &= \frac{\partial H}{\partial p}, \quad \dot{p} = -\frac{\partial H}{\partial x} \\ H(x, p, u) &= \max_{|v| \leq 1} H(x, p, v) \end{aligned}$$

with the boundary conditions

$$f(x(T)) = 0, \quad p(T) = p_0 \frac{\partial C}{\partial x} + \langle \xi, \frac{\partial f}{\partial x} \rangle, \quad p_0 \leq 0.$$

Moreover if the control is singular and non saturating, i.e. $|u_{1s}| < 1$, the generalized Legendre-Clebsch condition must hold:

$$\{\{H_1, H_0\}, H_1\} \geq 0. \quad (11)$$

2.5 Generic classification of the bang-bang extremals near the switching surface

An important issue in the contrast problem is to apply the results from [18] to classify the extremal curves near the switching surface. The switching surface is the set $\Sigma : H_1 = 0$, while the switching function is $t \mapsto \Phi(z(t)) = H_1(z(t))$, where $z(t)$ is an extremal curve. Let $\Sigma_s : H_1 = 0 = \{H_1, H_0\}$. The singular extremals are entirely contained in Σ_s . A bang-bang extremal $z(t)$ on $[0, T]$ is an extremal curve with a finite number of switching times $0 \leq t_1 < \dots < t_n \leq T$. We denote by ξ_+ , ξ_- the regular arcs for which $u = \pm 1$ and by ξ_s a singular arc; $\xi_1 \xi_2$ denotes an arc ξ_1 followed by an arc ξ_2 .

Ordinary switching time. It is a time t such that a bang-bang arc switches with the condition $\Phi(t) = 0$ and $\dot{\Phi}(t) = \{H_1, H_0\} \neq 0$. According to the maximum principle near Σ , the extremal is of the form $\xi_- \xi_+$ if $\dot{\Phi}(t) > 0$ and $\xi_+ \xi_-$ if $\dot{\Phi}(t) < 0$.

Fold case. It is the case where a bang arc has a contact of order 2 with the switching surface. Denoting $\ddot{\Phi}_\pm = \{\{H_1, H_0\}, H_0\} \pm \{\{H_1, H_0\}, H_1\}$ the second derivative of the switching function, if non zero, we have three cases:

1. *Hyperbolic case:* At the switching point, one has $\ddot{\Phi}_+ > 0$ and $\ddot{\Phi}_- < 0$. At Σ_s , a connection is possible with a singular extremal which is strictly admissible and satisfies the strong Legendre-Clebsch condition. The extremals are bang-singular-bang $\xi_\pm \xi_s \xi_\pm$.
2. *Elliptic case:* At the switching point, one has $\ddot{\Phi}_+ < 0$ and $\ddot{\Phi}_- > 0$. A connection with the singular extremal is not possible and every extremal curve is bang-bang but with no uniform bound on the number of switchings.
3. *Parabolic case:* It is the situation where $\ddot{\Phi}_+$ and $\ddot{\Phi}_-$ have the same sign at the switching point. One can check that the singular extremal is not admissible and every extremal curve near the switching point is bang-bang with at most two switchings, i.e. $\xi_+ \xi_- \xi_+$ or $\xi_- \xi_+ \xi_-$.

2.6 The concept of conjugate points in the affine case

According to [4], this concept is related to the notion of conjugate points in the regular case using the Goh reduction. The important property is the following geometric characterization. Let $z(\cdot) = (x(\cdot), p(\cdot))$ be a singular extremal associated to the control defined by (8). Assuming that it is strictly admissible, one can embed the singular extremal into a surface S formed by all the singular extremals starting from $x_0 = \Pi(z(0))$ and with initial adjoint vector p such that $|p - p(0)| \leq \varepsilon$. Up to the first conjugate point, the extremal synthesis is bang-singular-bang $\xi_{\pm} \xi_s \xi_{\pm}$, where bang arcs will be in the neighborhood of the reference singular extremal, which is related to the problem of extremizing the transfer time and hence to the Mayer problem. This synthesis is also valid in a C^0 -neighborhood of the reference case in the limit situation where $m \rightarrow +\infty$, m being the control bound.

2.7 Application to the contrast problem

A direct application is the contrast problem with the boundary condition $q_1(T) = 0$ and the cost $|q_2(T)|^2$. Splitting the adjoint vector into $p = (p_1, p_2)$, we deduce the transversality condition $p_2(T) = -2p_0 q_2(T)$, $p_0 \leq 0$. The case $p_0 = 0$ gives $p_2(T) = 0$. Since the system splits into:

$$\dot{q}_1 = F'_1(q_1, u), \quad \dot{q}_2 = F'_2(q_2, u)$$

the adjoint system decomposes into:

$$\dot{p}_1 = -p_1 \frac{\partial F'_1}{\partial q_1}, \quad \dot{p}_2 = -p_2 \frac{\partial F'_2}{\partial q_2}$$

where $p = (p_1, p_2)$ is written as a row vector. The condition $p_2(T) = 0$ corresponds to a second spin which is not controlled. In the non trivial case, p_0 is non zero and it can be normalized to $p_0 = -1/2$.

2.8 The embedding results

From the previous results, one deduces the following propositions.

Proposition 5 *The time minimizing solutions of the first spin 1/2 particle can be embedded as extremals of the contrast problem, with $p_0 = 0$.*

Proposition 6 *In the contrast problem, the extremals of the single-input case are extremals of the bi-input case.*

3 The single spin 1/2 case

Since in the contrast problem, the magnetization vector of the first particle has to be set to 0, an important issue is to analyze this task and the underlying problem of reaching this target in minimum time. Besides, the optimal solutions of such a problem can be embedded into the extremal solutions of the contrast problem. Indeed, if the transfer time in the contrast problem is exactly this minimum time, they are the only solutions satisfying the boundary conditions. Hence, in this section, based on the preliminary work [19], we make a thorough analysis of the single input case, with an emphasis put on the role of singular trajectories.

3.1 Preliminaries

First of all, since the initial condition is on the z - axis of revolution of the system, the control problem can be restricted to the 2D- meridian of the Bloch ball and the control field reduced to only one component [5, 7]. The system is $\dot{q} = F_0(q) + u_1 F_1(q)$, $|u_1| \leq m$, where

$$\begin{aligned} F_0 &= -\Gamma y \frac{\partial}{\partial y} + \gamma(1-z) \frac{\partial}{\partial z} \\ F_1 &= -z \frac{\partial}{\partial y} + y \frac{\partial}{\partial z}. \end{aligned}$$

Denoting $\delta = \gamma - \Gamma$, the following Lie brackets are relevant in our analysis:

$$\begin{aligned} [F_1, F_0] &= (-\gamma + \delta z) \frac{\partial}{\partial y} + \delta y \frac{\partial}{\partial z} \\ [[F_1, F_0], F_0] &= (\gamma(\gamma - 2\Gamma) - \delta^2 z) \frac{\partial}{\partial y} + \delta^2 y \frac{\partial}{\partial z} \\ [[F_1, F_0], F_1] &= 2\delta y \frac{\partial}{\partial y} + (\gamma - 2\delta z) \frac{\partial}{\partial z}. \end{aligned}$$

3.2 Singular trajectories and optimality

The singular trajectories are located on the set $S : \det(F_1, [F_1, F_0]) = 0$, which is given in our case by $y(-2\delta z + \gamma) = 0$. Hence it is formed by the z - axis of revolution $y = 0$ and the horizontal direction $z = \gamma/(2\delta)$. The singular control is given by $D' + u_{1s} D = 0$ where $D = \det(F_1, [[F_1, F_0], F_1])$ and $D' = \det(F_1, [[F_1, F_0], F_0])$.

- For $y = 0$, one has $D = -z(\gamma - 2\delta z)$ and $D' = 0$. The singular control is zero and the singular arc is solution of

$$\dot{y} = -y, \quad \dot{z} = \gamma(1-z)$$

where the equilibrium point $(0, 1)$ is stable if $\gamma \neq 0$.

- For $z = \gamma/(2\delta)$, $D = -2\delta y^2$, $D' = y\gamma(2\Gamma - \gamma)$ and $u_{1s} = \gamma(2\Gamma - \gamma)/(2\delta y)$, $2\Gamma - \gamma \geq 0$. Hence along the horizontal direction, the flow is

$$\dot{y} = -\Gamma y - \frac{\gamma^2(2\Gamma - \gamma)}{4\delta^2 y},$$

and $|u_{1s}| \rightarrow +\infty$ when $y \rightarrow 0$.

More precisely, along the horizontal singular line, the following proposition is crucial.

Proposition 7 *If $\gamma \neq 0$, the singular control along the horizontal singular line is in the L^1 but not in the L^2 - category, near $y = 0$.*

This can be straightforwardly shown by using the relations:

$$\int_{t_0}^{t_1} u_{1s}(t)^2 dt = \int_{y_0}^0 u_{1s}(y) \frac{dy}{\dot{y}} \quad (12)$$

where t_0 and t_1 are the initial and final times along the singular arc and y_0 the initial y - coordinate of this arc. One deduces that the integrand of Eq. (12) scales as $1/y$ when $y \rightarrow 0$ and that the corresponding integral has a logarithmic divergence.

In order to study the optimality of the singular directions, one uses the generalized Legendre-Clebsch condition, which takes the following form for a 2D-system. Let $D'' = \det(F_1, F_0) = \gamma z(z - 1) + \Gamma y^2$. The set $C = \{D'' = 0\}$ is the collinearity set. If $\gamma \neq 0$, this set is not reduced to a point and the intersection with the horizontal singular line is empty, except in the case $\gamma = 2\Gamma$. Singular lines are fast if $DD'' > 0$ and slow if $DD'' < 0$.

To complete the optimality analysis, one introduces the clock form $\omega = pdq$ which is defined outside the collinearity set C by the relations $\langle p, F_0 \rangle = 1$ and $\langle p, F_1 \rangle = 0$, the sign of $d\omega$ being given by $y(\gamma - 2\delta z)$. This form allows to deduce the optimality of singular extremals and to compare two different regular extremals when they do not cross the singular and collinearity sets [4].

Parameters conditions

The interesting case is when the horizontal singular line $z_0 = \gamma/(2\delta)$ cuts the Bloch ball $|q| \leq 1$, which gives the condition $\Gamma > 3\gamma/2$ and $-1 < z_0 < 0$. Using the generalized Legendre-Clebsch condition, one deduces that the horizontal line is optimal and the z - axis of revolution is optimal if $1 > z > z_0$. In particular, this line is slow in the domain $z_0 > z > -1$. Using the clock form, one can deduce that near the origin, the broken singular arc formed by a horizontal arc followed by a vertical line is time-minimal for the unbounded case, provided admissible controls are extended to L^1 . Note also that such a broken singular trajectory is not in L^2 and is not optimal for the energy minimization problem [6].

Having made this optimality analysis, one can deduce the time minimal optimal synthesis near the origin which is introduced next.

3.3 The SiSi singularity (Interaction between two singular arcs)

Assume $\gamma \neq 0$, $\Gamma > \frac{3}{2}\gamma$, $|u_1| \leq m$ and the control bound is large enough such that the bang arc $u_1 = m$ starting from the north pole $(0, 1)$ intersects the horizontal singular arc $z_0 = \gamma/(2\delta)$ at a point A. The horizontal singular line is admissible up to a saturating point B. The time minimal synthesis, with initial point A, is represented on Fig. 1. Due to the saturation phenomenon at B, there is a birth of a switching locus Σ_3 , but the remarkable fact due to the interaction between the horizontal and the vertical fast singular directions is the following concept.

Definition 5 *We call bridge between the horizontal singular arc and the vertical singular one, the bang arc, such that the concatenation singular-bang-singular is optimal.*

This concept is important and leads to a generalization in higher dimension, which plays an important role in the contrast problem.

In order to compute the global optimal synthesis provided m is large enough, we must analyze the synthesis near the north pole, which is presented next.

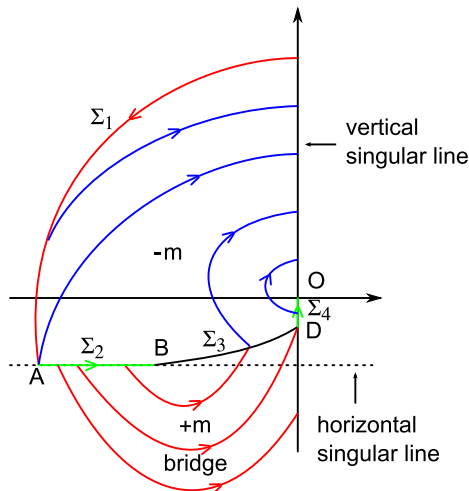


Figure 1: Schematic representation of the optimal synthesis when the initial point of the dynamics is the north pole. An arbitrary zoom has been used to construct the figure. Regular curves are plotted in blue (dark) and red (dark grey) for control fields equal to $-m$ and $+m$, respectively. The optimal singular trajectories are displayed in green (light grey). The black line is the switching curve, while the dashed one is the non-admissible part of the horizontal singular line.

3.4 The SiCo singularity (Interaction between the collinear set and the singular set)

Observe that the north pole is a stable fixed point for the free motion and the vertical singular direction is a fast direction, near the north pole, provided $z < 1$, as a consequence of the strong Legendre-Clebsch condition. The collinear set C corresponds to an oval below the line $z = 1$. Using polar coordinates $y = r \sin \phi$, $z = r \cos \phi$, one gets

$$r \frac{dr}{dt} = -\Gamma y^2 - \gamma(z - 1) = -D''.$$

Hence, r which represents the purity of the quantum system decreases outside the oval and increases inside. The north pole is a singularity of the optimal problem which combines a collinear situation with a singular one, but the analysis of the time-minimal synthesis near this point is simple because of the symmetry of revolution. Indeed, the only way to leave this singularity is to use a bang arc $u = \pm m$, which gives a boundary arc of the accessibility set. This first bang arc is followed by another bang arc $u = \mp m$ to fill the interior of the domain and to reach the vertical singular axis. This gives an optimal bang-bang policy (see the top part of Fig. 1).

3.5 The global synthesis

Under our assumptions ($\Gamma > 3\gamma/2 > 0$, m large enough), the global time minimal synthesis starting from the north pole is easily obtained gluing the two

previous syntheses (the one associated to the SiSi case with the one of the SiCo case). It is represented on Fig. 1. The switching locus is formed by the arc starting from the north pole and reaching the horizontal singular arc at A (it is denoted Σ_1 in the figure), the horizontal singular segment Σ_2 between the points A and B, the switching locus Σ_3 due to the saturation phenomenon and the part of the vertical singular direction between D and 0 (the Σ_4 segment), D being the extremity of the bridge. The bang arc with $u = -m$ starting from A is separating the two domains, one with a bang-bang policy and the other containing a non trivial singular arc.

At the limit, when $m \rightarrow +\infty$, it gives the synthesis constructed in Ref. [19] where the total time to reach the origin is formed by the time to follow the broken singular-singular arc between A and 0. Observe also that according to our analysis, the usual policy in NMR, the inversion recovery sequence, where only the vertical singular arc is used, is slow if $z < z_0$.

Also, note that the switching locus has a complicated structure, but due to the symmetry of revolution, all the cut points, i.e. the first points where the extremal trajectories cease to be optimal, are on the vertical z - axis where two symmetric solutions starting respectively on the left and right part of the Bloch disk intersect at the same time.

4 Preliminary results in the contrast problem

As mentioned in the introduction, the goal of the contrast problem is to bring the magnetization vector of spin 1 towards the center of the Bloch ball together maximizing the modulus of the magnetization vector of the other specie. Note that such a computation could have potential applications in magnetic resonance imaging in order to optimize the contrast of a given imaging [8, 9]. Roughly speaking, the species with a zero magnetization will appear dark, while the other species with a maximum modulus of the magnetization vector will be white. We introduce in the following a simple model reproducing the main features of this control problem. We describe the general structure of the optimal solution and we compute them for two particular examples.

4.1 The model system

Each spin 1/2 particle is governed by the Bloch equation:

$$\begin{aligned}\frac{dM_x}{dt} &= -\frac{M_x}{T_2} + \omega_y M_z \\ \frac{dM_y}{dt} &= -\frac{M_y}{T_2} - \omega_x M_z \\ \frac{dM_z}{dt} &= \frac{(M_0 - M_z)}{T_1} + \omega_x M_y - \omega_y M_x\end{aligned}$$

where the state variable is the magnetization vector and T_1, T_2 are the relaxation times. The control is the magnetic field $\omega = (\omega_x, \omega_y)$ which is bounded by $|\omega| \leq \omega_{max}$. We use the normalization introduced in [19]. The normalized coordinates are $q = (x, y, z) = (M_x, M_y, M_z)/M_0$. In these coordinates, the equilibrium point is the north pole $(0, 0, 1)$ and the normalized control is $u = (u_x, u_y) =$

$\frac{2\pi}{\omega_{max}}(\omega_x, \omega_y)$, $|u| \leq 2\pi$, while the normalized time is given by $\tau = \omega_{max}t/(2\pi)$. Hence the system takes the form:

$$\begin{aligned}\dot{x} &= -\Gamma x + u_y z \\ \dot{y} &= -\Gamma y - u_x z \\ \dot{z} &= \gamma(1-z) + (u_x y - u_y x)\end{aligned}$$

where $\Gamma = 2\pi/(\omega_{max}T_2)$ and $\gamma = 2\pi/(\omega_{max}T_1)$. In the experiments, ω_{max} can be chosen up to 15 000 Hz but the value $2\pi \times 32.3$ Hz will be considered in this paper. The experiments are done for the contrast problems of the cerebrospinal fluid/water [28] and the grey/white matter of cerebrum cases [10]. In the cerebrospinal fluid/water situation, the relaxation parameters for the first spin describing the fluid are $T_1 = 2000$ ms and $T_2 = 200$ ms, while for the second spin $T_1 = T_2 = 2500$ ms. In the second example, the rates of the grey matter are taken to be $T_1 = 920$ ms and $T_2 = 100$ ms, the rates for the white matter being $T_1 = 780$ ms and $T_2 = 90$ ms.

4.2 Computation of the singular flow

One restricts to the situation where the control field has only one component and the contrast problem is governed by the differential system $\dot{q} = F_0(q) + u_1 F_1(q)$, $q = (y_1, z_1, y_2, z_2)$:

$$\begin{aligned}F_0 &= \sum_{i=1}^2 [-\Gamma_i y_i \frac{\partial}{\partial y_i} + \gamma_i(1-z_i) \frac{\partial}{\partial z_i}] \\ F_1 &= \sum_{i=1}^2 (-z_i \frac{\partial}{\partial y_i} + y_i \frac{\partial}{\partial z_i}).\end{aligned}$$

Denoting $\delta_i = \gamma_i - \Gamma_i$, $i = 1, 2$ one has:

$$\begin{aligned}[F_1, F_0] &= \sum_{i=1}^2 (-\gamma_i + \delta_i z_i) \frac{\partial}{\partial y_i} + \delta_i y_i \frac{\partial}{\partial z_i} \\ [[F_1, F_0], F_0] &= \sum_{i=1}^2 [\gamma_i(\gamma_i - 2\Gamma_i) - \delta_i^2 z_i] \frac{\partial}{\partial y_i} + \delta_i^2 y_i \frac{\partial}{\partial z_i} \\ [[F_1, F_0], F_0] &= \sum_{i=1}^2 2\delta_i y_i \frac{\partial}{\partial y_i} + (\gamma_i - 2\delta_i z_i) \frac{\partial}{\partial z_i}\end{aligned}$$

and the corresponding singular flow is defined by:

$$H_1 = \{H_1, H_0\} = \{\{H_1, H_0\}, H_0\} + u_{1s} \{\{H_1, H_0\}, H_1\} = 0.$$

Since the equations are linear with respect to p , for each initial condition q_0 , this defines a two-dimensional surface $S(q_0)$ in the state space. An additional condition is provided by the generalized Legendre-Clebsch condition: $\{\{H_1, H_0\}, H_1\} \geq 0$. The structure of this surface is related to the relaxation parameters (Γ_i, γ_i) .

If the transfer time is not fixed, this leads to the additional constraints $H_0 = 0$. In this case, the singular flow defines a single vector field in the state

space, since the adjoint vector can be eliminated and the restricted singular control is given by:

$$u_{1s} = -\frac{D'(q)}{D(q)}$$

where

$$\begin{aligned} D'(q) &= \det(F_0, F_1, [F_1, F_0], [[F_1, F_0], F_0]) \\ D(q) &= \det(F_0, F_1, [F_1, F_0], [[F_1, F_0], F_1]) \end{aligned}$$

with the corresponding vector field

$$\frac{dq}{dt} = F_0(q) - \frac{D'(q)}{D(q)} F_1(q)$$

which can be analyzed using the time reparameterization $d\tau = dt/D(q(\tau))$. In this framework, singular trajectories are used to classify the systems.

In the general case, a similar computation shows that the singular trajectories are solutions of an equation of the form:

$$\frac{dq}{dt} = F_0(q) - \frac{D'(q, \lambda)}{D(q, \lambda)} F_1(q) \quad (13)$$

where λ is a one dimensional time dependent parameter whose dynamics is deduced from the adjoint equation. The solutions of Eq. (13) emanating from q_0 will form $S(q_0)$.

4.3 Numerical simulations on singular trajectories

We present some numerical simulations concerning the singular trajectories. The projection of $S(q_0)$ on the planes (y_1, z_1) , (y_2, z_2) shows the effect of the relaxation parameters on the contrast. This point is illustrated by the figures 2 and 3 for the cerebrospinal fluid/water and grey/white matter of cerebrum cases, respectively. In each example, we assume that a bang pulse of large amplitude has been first applied to the system, the initial point of the singular flow is of coordinates $((-\sqrt{1-z_0^2}, z_0), (-\sqrt{1-z_0^2}, z_0))$ where $z = z_0$ is the horizontal singular line of the first spin. This first bang is necessary so that the singular trajectory of the spin 1 can reach the center of the Bloch ball. One clearly sees in Fig. 3 the similar structure of the different singular trajectories of the two spins. The situation is completely different in Fig. 2 for the first example. This explains the excellent and weak contrasts that can be reached in the first and second examples with an optimal sequence of the form bang-singular. Note that some singular control fields diverge as displayed in Figs. 2 and 3. The conjugate points defined in Sec. 2 have been computed for each singular extremal as shown in Fig. 4. Similar results have been obtained for the spin 2 and for the grey/white matter case. This shows that the structure bang-singular is not optimal since the first conjugate point occurs before the saturation of the spin. A more complicated pulse sequence such as bang-singular-bang-singular has therefore to be used.

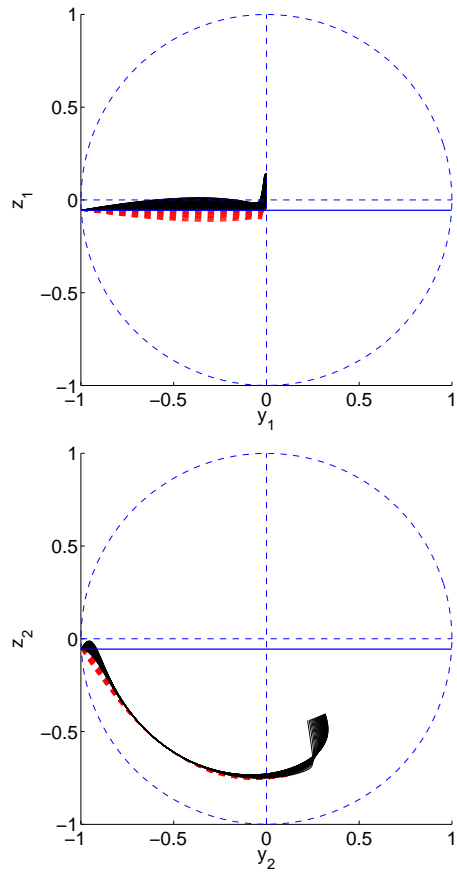


Figure 2: Structure of the projection of the singular flow onto the planes (y_1, z_1) and (y_2, z_2) in the cerebrospinal fluid/water case. The trajectories are plotted in black (solid line) and in red (dashed line). The control fields of the dashed extremals diverge. The trajectories have been plotted up to the explosion of the field (The absolute value of the field is larger than 10^5). The horizontal solid line is a singular line of the first spin.

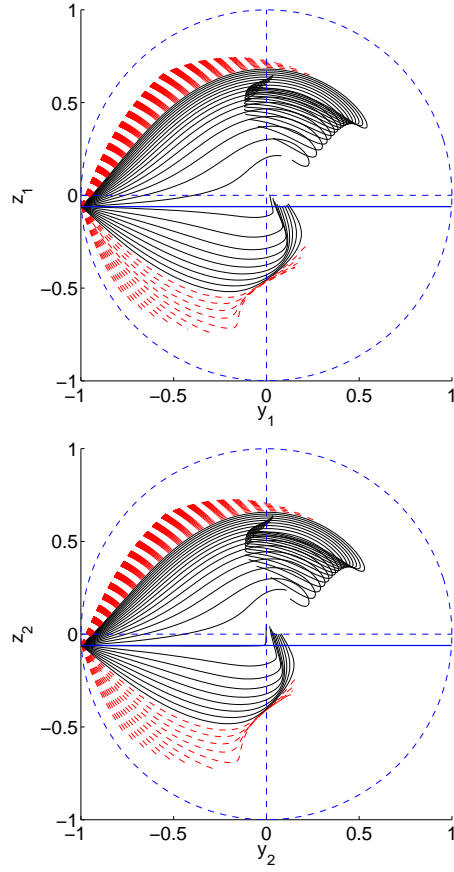


Figure 3: Same as Fig. 2 but for the grey/white matter case. An explosion of the control field is observed for the red trajectories.

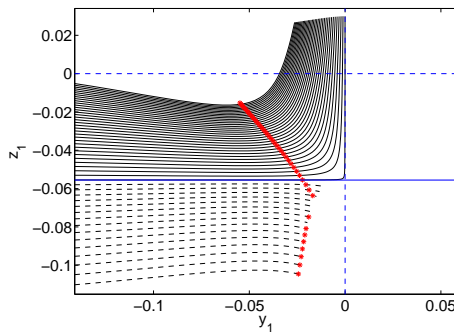


Figure 4: Zoom of the results of Fig. 2 for the spin 1 near the origin. The red crosses indicate the position of the first conjugate point. The dashed lines represent the singular trajectories for which the control field diverges.

4.4 Some preliminaries numerical results on the contrast problem

Due to the numerical difficulty of the computation of the bang-singular-bang-singular optimal sequence, we only present in this section some preliminary results. To make the numerical simulations, we have used a differential continuation method of the Hampath code [14] where the cost is regularized by adding a L^2 (or a $L^{2-\lambda}$) penalty on the control. Note that another continuation on the transfer time has also been used in the computations. Such results can be compared with the GRAPE algorithm [12, 16, 24, 25] which is a standard approach in NMR to solve the optimization problems.

In the first study, the cost is regularized as

$$C(x(T)) + (1 - \lambda) \int_0^T u^2(t) dt,$$

where λ is a continuation parameter and the transfer time varies starting from $T_{min} + \varepsilon$ to $2T_{min}$, where T_{min} is the minimum time to saturate the first spin and $\varepsilon \ll 1$ an arbitrary parameter. According to Sec. 3, in the limit case where $T = T_{min}$, the optimal solution of the contrast problem is exactly the solution of driving the first spin to the origin.

The different numerical results are presented in Figs. 5, 6, 7 and 8. The different behaviors for the two examples can be clearly seen since the best contrast $\sqrt{y_2^2(t) + z_2^2(t)}$ is of the order of 0.73 and 0.07 in the first and second examples, respectively. Note also that for $T = T_{min} + \varepsilon$, the trajectory of the spin 1 is very close to the trajectory for saturating this spin in minimum time.

An interesting phenomenon can be observed in the cerebrospinal fluid/water situation in Fig. 5, where there exists a bifurcation of the optimal policy when T increases. This is related to the introduction of a bang-bang policy associated to a SiCo singularity. Also we observe that the optimal policy is crossing the z_1 - axis of revolution. Further work is necessary to improve the continuation method near $\lambda = 1$ since the L^2 - regularization of the cost is not adapted to the control saturation that can be found in the SiSi singularity where the control is L^1 and not L^2 .

This point is illustrated by a second series of simulations where we have considered the following regularized cost:

$$C(x(T)) + (1 - \lambda) \int_0^T |u|^{2-\lambda}(t) dt$$

and as before a continuation has been performed on the control duration T . The computation has been done for $\lambda = 0.9$. Similar contrasts have been reached in this second situation. Note, however, the different peaks appearing in the evolution of u , to be compared to the first regularization.

We complete this paper by illustrating our numerical results on a simulated and a real contrast experiments. For the simulated experiment, we consider two surfaces as displayed in Fig. 11 filled in with spins 1 or 2 in a homogeneous manner. We apply the optimal control field and we associate a color to the final modulus of the magnetization vector of the spin 2. This color is white if the modulus is equal to 1, black if it is zero and a grey variant between. One clearly sees in Fig. 11 the excellent and weak contrasts that can be obtained in the first and second examples.

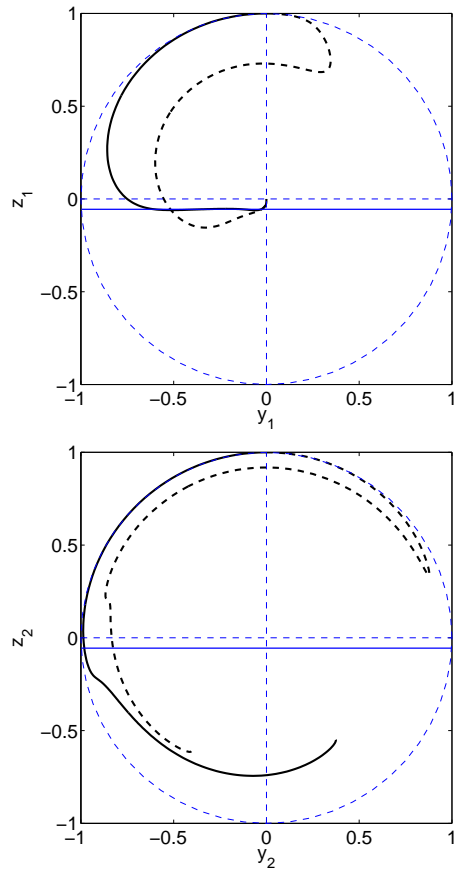


Figure 5: (The cerebrospinal fluid/water case) Trajectories of the first and second spins for $T_{min} + \varepsilon$ and $2T_{min}$ in solid and dashed lines, respectively. The horizontal singular line is plotted in solid line. The parameter λ is taken as 0.9.

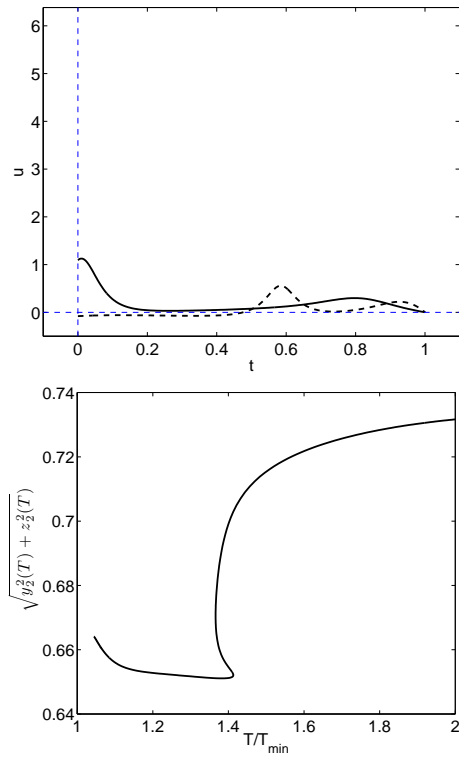


Figure 6: (top) Evolution of the control field associated to Fig. 5 for $T_{min} + \epsilon$ and $2T_{min}$ in solid and dashed lines, respectively. The time T has been normalized to 1 to plot the two control fields on the same figure. (bottom) Evolution of the contrast parameter $\sqrt{y_2(T)^2 + z_2(T)^2}$ as a function of the control duration.

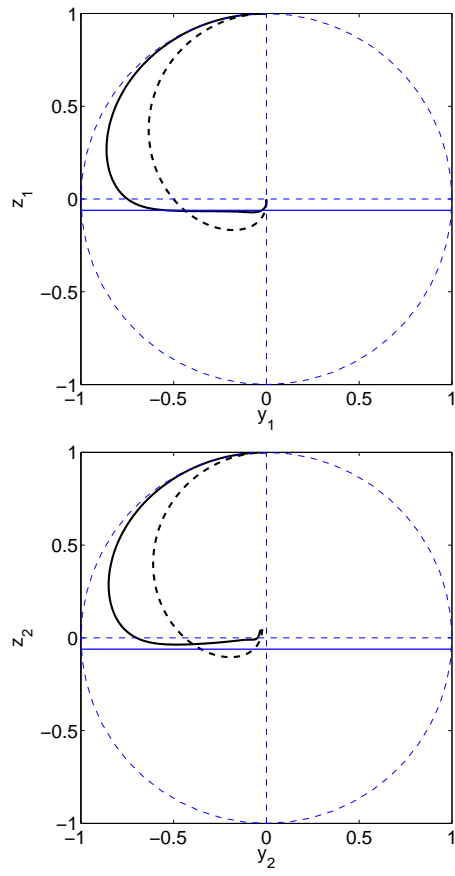


Figure 7: Same as Fig. 5 but for the grey/white matter of cerebrum.

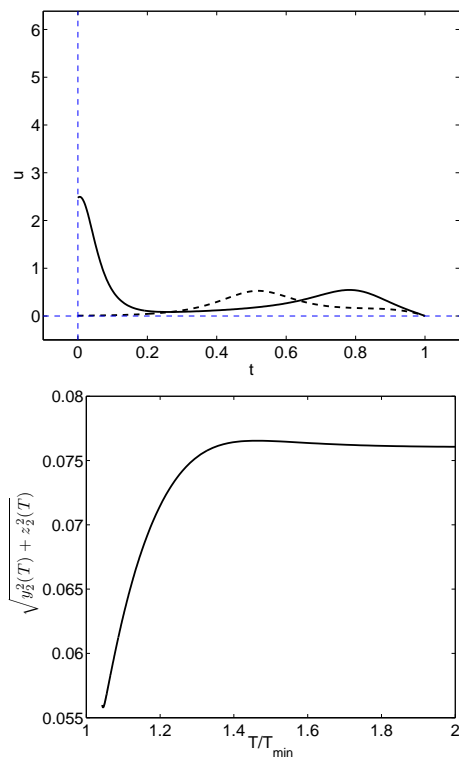


Figure 8: Same as Fig. 6 but for the grey/white matter of cerebrum.

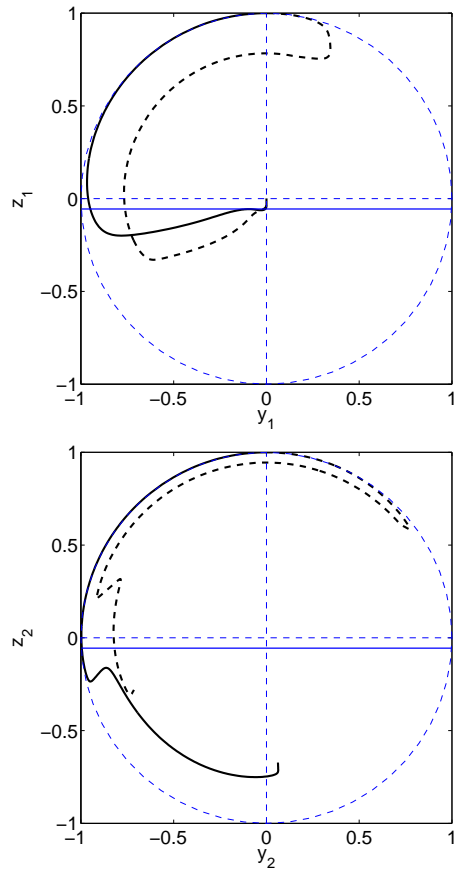


Figure 9: Same as Fig. 5 but for the second regularized cost functional. The parameter λ is taken as 0.93.

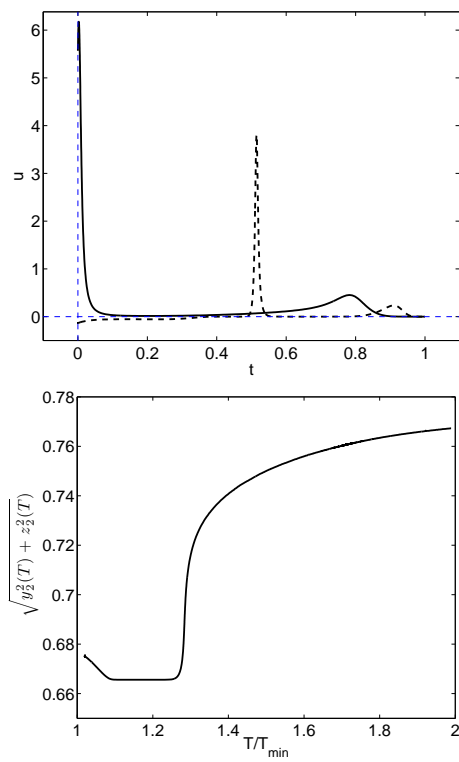


Figure 10: Same as Fig. 6 but for the second regularized cost functional.

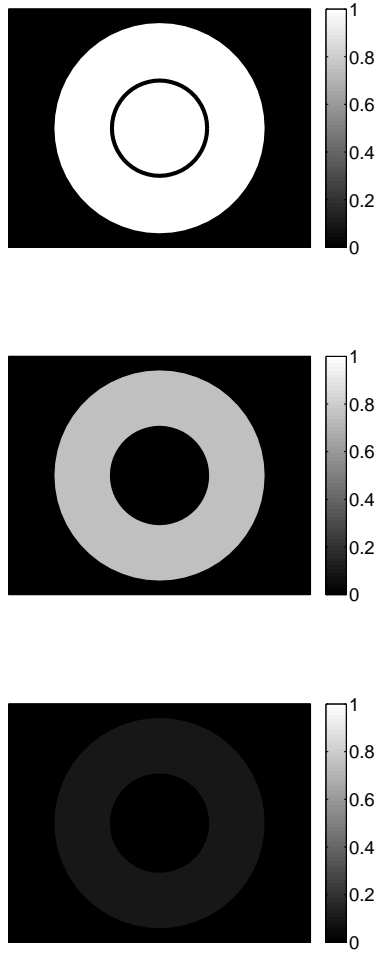


Figure 11: Simulated experimental results on the contrast problems of the cerebrospinal fluid/water (middle) and the grey/white matter of cerebrum (bottom) examples. The inner disk mimics the spin 1, while the outside ring mimics the spin 2. The two surfaces are separated by a thin black circle. The top figure is a reference image where a 90 degree pulse has been applied to the two spins. The middle and bottom images are a representation of the contrast as could be done in a real experiment. For these two images, the control sequence is the optimal field. A color has been associated to each value of the contrast between 0 and 1, 0 and 1 corresponding respectively to the colors black and white.

In Fig. 12, we compute by interpolation the contrast between the two spin particles for different values of the relaxation parameters. To have a 2-D representation, one fixes the first spin parameters. In the top figure, the first spin corresponds to the cerebrospinal fluid ($T_1^1 = 2000$ ms and $T_2^1 = 200$ ms), in the middle figure, it is the gray matter ($T_1^1 = 920$ ms and $T_2^1 = 100$ ms) and in the bottom one, it is the deoxygenated blood ($T_1^1 = 1350$ ms and $T_2^1 = 50$ ms), this latter example being illustrated below experimentally. In each case, we fix the control duration T to $1.5T_{min}$ and we choose the regularized cost $C(x(T)) + (1 - \lambda) \int_0^T |u|^{2-\lambda}(t)dt$, with $\lambda = 0.9$. We consider the following variations for the parameters of the second spin:

$$\begin{aligned} x_{min} &\leq T_1^2 \leq x_{max} \\ y_{min} &\leq T_2^2 \leq y_{max}, \end{aligned}$$

where $(x_{min}, x_{max}, y_{min}, y_{max}) = (80, 4000, 160, 4000)$ for the fluid case, $(45, 1500, 90, 1500)$ for the matter case and $(20, 2000, 40, 2000)$ for the blood case. The linear inequalities $T_2 \leq 2T_1$ due to the physical model, leads to convex polyhedrons in Fig. 12. The starting point of the forthcoming homotopies corresponds to $S = (T_1^1, T_2^1)$ for which the contrast is zero. Then we discretize the edges of the polytope P into n points and for each $F_k = (T_1^{2,k}, T_2^{2,k})$, $k = 1, \dots, n$, we perform a linear homotopy from S to F_k by introducing a parameter λ such that :

$$\begin{aligned} T_1^2 &= T_1^1 + \lambda(T_1^{2,k} - T_1^1) \\ T_2^2 &= T_2^1 + \lambda(T_2^{2,k} - T_2^1). \end{aligned}$$

At the end, we have n lines starting from S which mesh P and to complete the figures, we use a standard Matlab interpolation function. We can see in Fig. 12, on the top figure, that the contrast in $O = (2500, 2500)$, which corresponds to the Fluid/Water case, is nearly 0.7 and on the middle one, in $O = (780, 90)$, the Gray/White matter case, the contrast is almost 0.1, which agree with the results given in Figs. 10 and 8 respectively.

4.5 Some preliminary experimental results

The first experimental results on the contrast problem are represented on Fig. 13 and correspond to samples reproducing the case of the deoxygenated/oxygenated blood. Such results can be compared to Fig. 11 where they have been numerically simulated for other samples in an ideal experiment. The preliminary experimental results are promising even if some artefacts due to the inhomogeneities of the magnetic field deteriorate the quality of the image.

5 Conclusion

In the conclusion, we discuss some important issues related to our study.

Mathematical problems. The important remaining question is to analyze the dynamics of the singular flow in relation with the relaxation times and in particular the asymptotic of the trajectories.

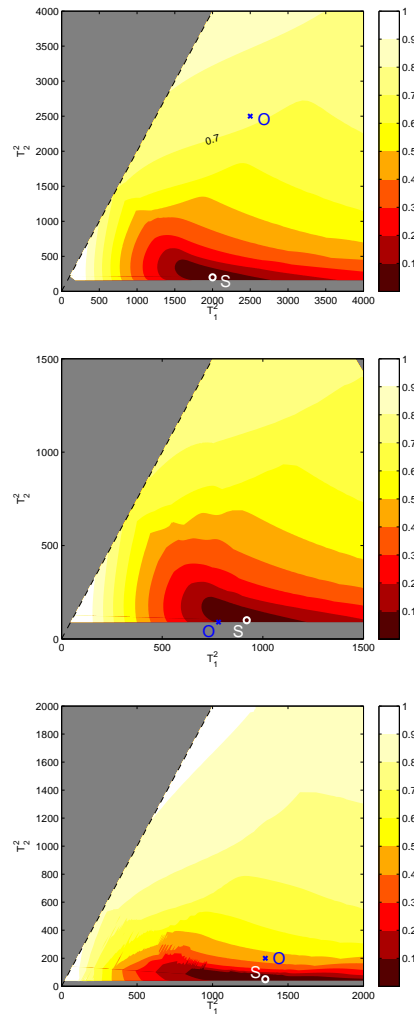


Figure 12: Interpolation results for the (top) Fluid case, the (middle) Gray matter case and the (bottom) Blood case. The contrast is computed with respect to the spin 2 relaxation parameters. The parameters of the spin 1 are fixed to the ones of the points S . The points O give us the contrast for known problems, as the fluid/water case on the top figure, gray/white matter case on the middle one and deoxygenated/oxygenated blood on the bottom figure.

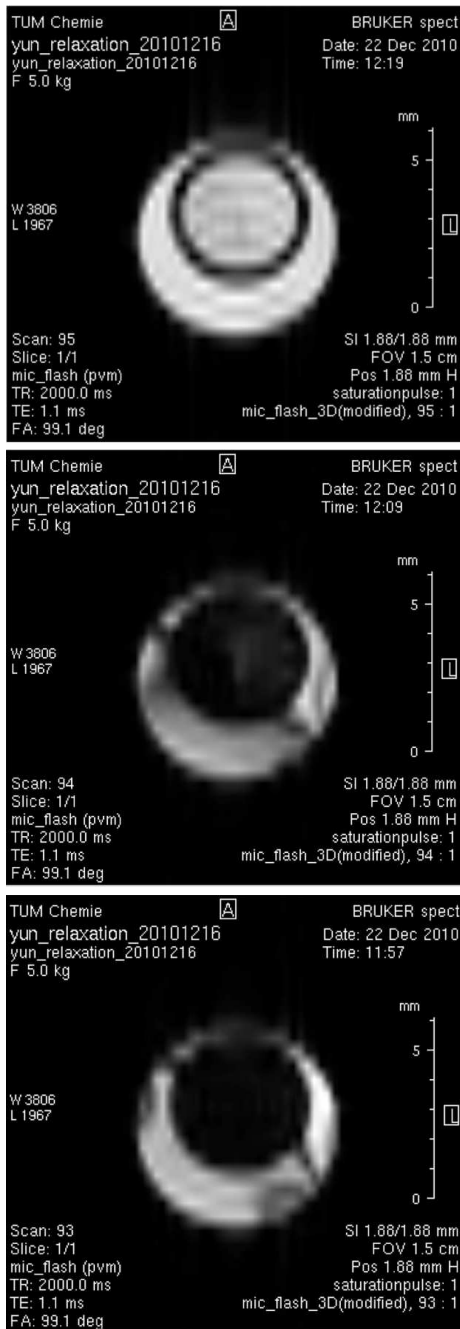


Figure 13: Experimental results: The inner circle shape sample mimics the deoxygenated blood, where $T_1 = 1.3$ s and $T_2 = 50$ ms; the outside moon shape sample corresponds to the oxygenated blood, where $T_1 = 1.3$ s and $T_2 = 200$ ms. The goal of the control is to saturate the inner sample and to maximize the remaining magnetization of the outside sample. The upper image is a reference image after a short 90 degree pulse on both samples. The image at the middle is the remaining Y magnetization $|M_y|$ after the optimized pulse, the lower image is the remaining Z magnetization $|M_z|$ after the optimized pulse.

Numerical problems. The main points consist of generating accurately complicated Bang-Singular sequences solutions of the Maximum Principle and to prove the convergence of the continuation problems. In this setting, the problem is to initialize the shooting equation using the continuation method.

Improving experimental results. The preliminary experimental figure 13 shows the problem of the magnetic fields inhomogeneities, which have therefore to be taken into account in the model. In this case, the geometric techniques can be used as a first step to initialize a purely iterative numerical approach such as the GRAPE algorithm [12, 16, 24, 25]. In this setting, the geometric solution provides an efficient initial solution and gives the physical limit of the contrast problem that can be reached. The GRAPE algorithm is then able to solve the simultaneous optimal control of a large number of spins of an inhomogeneous ensemble. In the example where the goal is to saturate the spins in deoxygenated blood, while maximizing the final magnetization of oxygenated blood, the numerically optimized pulse achieved about 93% and 70% of the contrast found by the optimal geometric solution for the ideal and the real cases. Note that this problem with magnetic field inhomogeneities is related to the controllability analysis of [3].

Acknowledgment.

B. B. and D. S acknowledge support from the PEPS INSIS *Optimal control of spin dynamics in Nuclear Magnetic Resonance Imaging*.

References

- [1] C. ALTAFINI, *Controllability properties for finite dimensional quantum Markovian master equations*, J. Math. Phys. **44**, 2357 (2002).
- [2] E. ASSÉMAT, M. LAPERT, Y. ZHANG, M. BRAUN, S. J. GLASER AND D. SUGNY, *Simultaneous time-optimal control of the inversion of two spin 1/2 particles*, Phys. Rev. A, **82**, 013415 (2010).
- [3] K. BEAUCHARD, J.-M. CORON AND P. ROUCHON, *Controllability issues for continuous-spectrum systems and ensemble controllability of Bloch equations*, Comm. Math. Phys. **296**, 525 (2010)
- [4] B. BONNARD AND M. CHYBA, *Singular trajectories and their role in control theory*, Math. and Applications 40, Springer-Verlag, Berlin (2003)
- [5] B. BONNARD, M. CHYBA AND D. SUGNY, *Time-minimal control of dissipative two-level quantum systems: The generic case*, IEEE Transactions A. C., **54**, 2598 (2009).
- [6] B. BONNARD, O. COTS, N. SHCHERBAKOVA AND D. SUGNY, *The energy minimization problem for two-level dissipative quantum systems*, J. Math. Phys., **51**, 092705 (2010)
- [7] B. BONNARD AND D. SUGNY, *Time-minimal control of dissipative two-level quantum systems: The integrable case*, SIAM J. Control Optim., **48**, 1289 (2009).

- [8] G. M. BYDDER, J. V. HAJNAL AND I. R. YOUNG, *MRI: Use of the inversion recovery pulse sequence*, *Clinical Radiology*, **53**, 159 (1998)
- [9] M. CARL, M. BYDDER, J. DU, A. TAKAHASHI AND E. HAN, *Optimization of RF excitation to maximize signal and T_2 contrast of tissues with rapid transverse relaxation*, *Magnetic Resonance in Medicine*, **64**, 481 (2010)
- [10] K. V. R. CHARY AND G. GOVIL, *NMR in biological systems, from molecules to human*, Focus on structural biology, vol. 6, Springer (2008)
- [11] R. R. ERNST, *Principles of Nuclear Magnetic Resonance in one and two dimensions* (International Series of Monographs on Chemistry, Oxford University Press, Oxford, 1990)
- [12] N. I. GERSHENZON, K. KOBZAR, B. LUY, S. J. GLASER AND T. E. SKINNER, *Optimal control design of excitation pulses that accomodate relaxation*, *J. Magn. Reson.* **188**, 330 (2007)
- [13] V. GORINI, A. KOSSAKOWSKI AND E. C. G. SUDARSHAN, *Completely positive dynamical semigroups of N -level systems*, *J. Math. Phys.*, **17**, 821 (1976).
- [14] <http://apo.enseiht.fr/hamopath>
- [15] N. KHANEJA, R. BROCKETT AND S. J. GLASER, *Time optimal control in spin systems*, *Phys. Rev. A*, **63**, 032308 (2001).
- [16] N. KHANEJA, T. REISS, C. KEHLET, T. SCHULTE-HERBRÜGGEN AND S. J. GLASER, *Optimal control of coupled spin dynamics: Design of NMR pulse sequences by gradient ascent algorithms*, *J. Magn. Reson.* **172**, 296 (2005).
- [17] A. J. KRENER, *The high order maximal principle and its application to singular extremals*, *SIAM J. Control Optimization*, **15**, 2, 256 (1977)
- [18] I. KUPKA, *Geometric theory of extremals in optimal control problems. I. The fold and Maxwell case*, *Trans. Amer. Math. Soc.* **299**, 1, 225 (1987)
- [19] M. LAPERT, Y. ZHANG, M. BRAUN, S. J. GLASER AND D. SUGNY, *Singular extremals for the time-optimal control of dissipative spin 1/2 particles*, *Phys. Rev. Lett.*, **104**, 083001 (2010)
- [20] M. H. Levitt 2008 *Spin dynamics: basics of nuclear magnetic resonance* (John Wiley and sons, New York-London-Sydney)
- [21] G. LINDBLAD, *On the generators of quantum dynamical semi-groups*, *Comm. Math. Phys.*, **48**, 119 (1976).
- [22] M. MIRRAHIMI AND P. ROUCHON, *Singular perturbations and Lindblad-Kossakowski differential equations*, *IEEE Trans. Automatic Control*, **54**, 6, 1325 (2009)
- [23] L. PONTRYAGIN ET AL, *Théorie mathématique des processus optimaux*, Mir, Moscow, 1974.

- [24] T. E. SKINNER, T. O. REISS, B. LUY, N. KHANEJA AND S. J. GLASER, *Application of Optimal Control Theory to the Design of Broadband Excitation Pulses for High Resolution NMR*, J. Magn. Reson. **163**, 8 (2003)
- [25] T. E. SKINNER, T. O. REISS, B. LUY, N. KHANEJA AND S. J. GLASER, *Tailoring the optimal control cost function to a desired output: Application to minimizing phase errors in short broadband excitation pulse*, J. Magn. Reson. **172**, 17 (2005)
- [26] D. SUGNY, C. KONTZ AND H. R. JAUSLIN, *Time-optimal control of a two-level dissipative quantum system*, Phys. Rev. A, **76**, 023419 (2007).
- [27] T. VIELLARD, F. CHAUSSARD, D. SUGNY, B. LAVOREL AND O. FAUCHER, *Field-free molecular alignment of CO₂ mixtures in presence of collisional relaxation*, J. Raman Spec., **39**, 694 (2008).
- [28] C. WESTBROOK AND C. ROTH, *MRI in practice* (3rd Edition), Blackwell Publishing Ltd. (2005)
- [29] Y. ZHANG, M. LAPERT, M. BRAUN, D. SUGNY AND S. J. GLASER, *Time-optimal control of spin 1/2 particles in presence of relaxation and radiation damping effects*, J. Chem. Phys. **134**, 054103 (2011)